

The contribution of long-period stacking-ordered structure (LPSO) to high strength-high ductility combination and nanoscale deformation behavior of magnesium-rare earth alloy

K. Li, V.S.Y. Injeti, R.D.K. Misra, L.G. Meng, X.G. Zhang



PII: S0921-5093(17)31653-2  
DOI: <https://doi.org/10.1016/j.msea.2017.12.056>  
Reference: MSA35898

To appear in: *Materials Science & Engineering A*

Received date: 23 August 2017  
Revised date: 4 November 2017  
Accepted date: 13 December 2017

Cite this article as: K. Li, V.S.Y. Injeti, R.D.K. Misra, L.G. Meng and X.G. Zhang, The contribution of long-period stacking-ordered structure (LPSO) to high strength-high ductility combination and nanoscale deformation behavior of magnesium-rare earth alloy, *Materials Science & Engineering A*, <https://doi.org/10.1016/j.msea.2017.12.056>

This is a PDF file of an unedited manuscript that has been accepted for publication. As a service to our customers we are providing this early version of the manuscript. The manuscript will undergo copyediting, typesetting, and review of the resulting galley proof before it is published in its final citable form. Please note that during the production process errors may be discovered which could affect the content, and all legal disclaimers that apply to the journal pertain.

**The contribution of long-period stacking-ordered structure (LPSO)  
to high strength-high ductility combination and nanoscale deformation  
behavior of magnesium-rare earth alloy**

K. Li<sup>1</sup>, V.S.Y. Injeti<sup>1</sup>, R.D.K. Misra<sup>1\*</sup>, L.G. Meng<sup>2</sup>, X.G. Zhang<sup>2</sup>

<sup>1</sup>Department of Metallurgical, Materials and Biomedical Engineering,  
University of Texas at El Paso  
500 W. University Avenue  
El Paso, TX 79968-0521, USA

<sup>2</sup>School of Materials Science and Engineering,  
Dalian University of Technology, Dalian, 116024, China

### Abstract

The nanoscale deformation behavior of high strength (240 MPa)-high ductility (21.4%) combination Mg-rare earth alloy with long-period stacking-ordered structure was studied via nanoindentation and electron microscopy, and the behavior compared with the low strength (65 MPa)-good ductility (15%) alloy without LPSO structure. In non-LPSO alloy, basal  $\langle a \rangle$  slip mainly occurred, while in LPSO-containing alloy, the LPSO changed the deformation mechanism to extensive non-basal  $\langle c+a \rangle$  slip and deformation twinning. The intrinsic good plasticity of LPSO and its impact on the deformation mechanism of Mg matrix contributed to superior mechanical properties and nanoscale deformation behavior of Mg-rare earth alloys, without compromising the ductility.

**Keywords:** long-period stacking-ordered structure (LPSO); nanoscale deformation behavior; deformation mechanism; magnesium-rare earth alloy

## 1. Introduction

Magnesium and its alloys have significant potential as structural and functional materials in aerospace, automotive and biomedical applications, because of low density, good damping capacity, biodegradable and biocompatible characteristics [1-3]. However, low strength and poor room temperature formability of magnesium alloys restrict their use for structural applications [4,5]. Thus, a significant effort is being devoted to enhance the strength and ductility of magnesium alloys [6]. Recently, magnesium alloys containing Mg-TM (transition-metal)-RE (rare-earth elements) ternary precipitates with long-period stacking-ordered (LPSO) structures have attracted considerable attention [7-9]. It is reported that LPSO structures can improve both strength and elongation at elevated temperature because of excellent thermal stability and ability to withstand deformation [10,11]. Therefore, the current interest is to understand their crystal structure, and their impact on mechanical properties and deformation mechanisms.

The LPSO structures include 6H, 10H, 14H, 18R and 24R types [12-15]. LPSO phase may increase the critical resolved shear stress (CRSS) of basal plane and promote the activation of non-basal plane slip [16], based on the predictions of first principle calculations [17]. On the contrary, Hagihara et al. proposed that  $\langle a \rangle$  basal slip and deformation kinks were the dominant deformation in compression deformation for both 14H-type and 18R-type LPSO phase and the CRSS of basal slip was decreased to 10-30 MPa [18,19]. While Shao et al. observed kink bands instead of non-basal slip in LPSO-containing alloys, which was proposed to improve the yield strength via suppression of  $\langle a \rangle$  basal slip [20]. However, recent studies suggest that the deformation mode of LPSO is kink-bands, while magnesium matrix deformed by pyramidal  $\langle c+a \rangle$  slip or deformation twinning [21,22]. But an in-depth analysis of the deformation mechanism and the underlying reasons for the different deformation behavior was not given. In

summary, the role of LPSO phase on the deformation mechanism of Mg-RE alloys continues to be fragmented. Thus, the objective of the present study is to elucidate the determining role of LPSO in impacting the deformation behavior of Mg-RE alloys. The objective was accomplished by studying two different chemical compositions of Mg-RE alloys in the presence and absence of Zn, where the presence of Zn promotes the formation of LPSO structures.

## 2. Materials and experimental procedure

The nominal chemical composition of LPSO-free Mg alloy was Mg-3Gd-1.7Y-0.5Zr (wt.%) (referred as M1 alloy), while that of LPSO-containing alloy had an additional 2 wt.% Zn (referred as M2 alloy). The alloy design is based on the knowledge that Gd and Y have high solid solubility in Mg and provide significant solid solution strengthening, Zr facilitates grain refinement, and Zn promotes the formation of LPSO when Gd and Y are present [23,24]. The as-cast alloy ingots were prepared by melting 99.85 wt-%Mg, 99.9 wt-%Zn, 99.85 wt-%Y and binary Mg-30 wt-%Gd and Mg-30 wt-%Zr master alloys in an electric resistance furnace under antioxidising flux. The melt was poured in a 300°C preheated steel mold and cooled to room temperature. The as-cast Mg-RE alloy samples were cut into 5 mm × 5 mm × 5 mm dimensions and metallographically polished to mirror finish. The samples were etched for ~30-60 s in a solution containing 8 g picric acid, 5 ml acetic acid, 10 ml distilled water, and 100 ml ethanol for microstructural observations by light microscopy. The electropolishing solution for SEM examination consisted of ethanol, perchloric acid and glycerin in the ratio of 8.5:1:0.5 at a voltage of 25V for 30s. Transmission electron microscopy studies were carried out on 3 mm disks that were electropolished in a solution containing 3% perchloric acid in ethanol using a Hitachi H-9500 TEM operated at 300 kV accelerating potential.

To study the microstructural evolution during deformation, nanoindentation experiments were carried out, followed by post-mortem transmission electron microscopy of the plastic zone surrounding the nanoindentation. The following procedure was adopted. First, 3 mm disks were punched from the polished thin samples. To ensure that the nanoindents are distributed along the thin area of the disk for examination in TEM, a modification of twin-jet electropolishing and a new design of sample mounting for nanoindentation was developed and is described previously [25]. Nanoindentation experiments were carried out in load-controlled mode with a constant loading rate of 2  $\mu\text{N/s}$ , with maximum load set to 0.5 mN using MTS Nanoindenter system with a Berkovich three-sided pyramidal diamond indenter with a nominal angle of  $65.3^\circ$  and indenter diameter of 20 nm. An array of indents of matrix  $10 \times 10$  were defined with the indent gap of 10  $\mu\text{m}$ . After the indentation experiments, the disks were removed from the mount and electropolishing was carried out only from the side opposite to the indented surface. The disks were partially jet electropolished in a refrigerated electrolyte of 3% perchloric acid in ethanol at 30 V for ~30 s to obtain a shining surface in the center part of the 3 mm disk. Using this procedure, the area surrounding the indents, which is present along the jet-polished hole was electron transparent to study the deformation behavior using TEM. Tensile properties were measured at room temperature via WD-10A universal tensile testing equipment at a strain rate of  $1 \times 10^{-3} \text{ s}^{-1}$ .

The data presented in the manuscript was carefully analyzed and checked for excellent reproducibility of the “indentation-induced deformation structures” and “TEM morphologies”. We carried out a number of experiments for each sample, followed by extensive TEM studies on at least 5 foils for each sample.

### 3. Results and discussion

Fig. 1 shows the microstructure of as-cast M1 (free of LPSO) and M2 (LPSO-containing) alloys. No precipitates, dislocations or LPSO were present in the matrix of M1 alloy with an average grain size of 150  $\mu\text{m}$  (Fig. 1a). In M2 alloy, the average grain size was 75  $\mu\text{m}$  and the secondary phase was discontinuously distributed along the grain boundaries (Fig. 1b(i)). The secondary phase was comprised of acicular and lamellar layers (Fig. 1b(ii)). To study the crystal structure of the secondary phase, TEM bright field image and corresponding selected area diffraction pattern of the lamellar phase are presented in Fig. 1c. The secondary lamellar phase was identified to be 18R LPSO [ $\text{Mg}_{12}\text{Zn}(\text{Y},\text{Gd})$ ], as illustrated by the selected area diffraction pattern in Fig. 1c(ii) and was also confirmed by X-ray diffraction (Fig. 2). In Fig. 1c(ii), the  $c^*$  axis of the diffraction pattern is perpendicular to the lamellar phase, which further confirmed the presence of LPSO. Comparing the chemical composition of M1 and M2 alloys, the underlying reason for the formation of LPSO structure is the element, Zn [24].

The mechanical properties of M1 and M2 alloys are listed in Table 1. The M2 alloy with LPSO structure had excellent combination of strength and ductility (yield strength: 131 MPa, ultimate strength: 240 MPa, elongation: 21.4%), compared to M1 alloy (yield strength: 32 MPa, ultimate strength: 65 MPa, elongation: 15%). This clearly indicates that LPSO structure enhances both strength and elongation and is likely to have a significant effect on the deformation mechanism of Mg-RE alloys.

To study the influence of LPSO structure on the deformation mechanism of Mg-RE alloys, post-mortem TEM analysis of plastic zone surrounding the indentation in M1 and M2 alloys was conducted, as presented in Figs. 3 and 4, respectively. In this study, both the as-cast alloys were processed under identical conditions and no apparent texture was observed. In the case of M1

alloy, the presence of dislocations was not apparent in zone A, which is far from indentation, while a number of dislocations were present in zone B in the vicinity of indentation (Fig. 3a). At high magnification, a number of short and bent dislocation lines were observed in the two-beam condition of  $g = [10\bar{1}0]$ . These dislocations totally disappeared when  $g$  vector was changed to  $g = [0002]$ . It is known that  $\langle a \rangle \frac{1}{3} \langle 11\bar{2}0 \rangle$  dislocations, which include basal  $\langle a \rangle$ , prismatic  $\langle a \rangle$  and the first order pyramidal  $\langle a \rangle$ , are invisible in the two-beam condition of  $g = [0002]$ . While pyramidal  $\langle c+a \rangle$  dislocations cannot completely disappear in the two-beam condition of  $g = [0002]$ . Thus, this dislocation must be  $\langle a \rangle \frac{1}{3} \langle 11\bar{2}0 \rangle$  dislocation. It is proposed that the critical resolved shear stress (CRSS) follows the relationship:  $CRSS_{\text{basal}} < CRSS_{\text{twinning}} < CRSS_{\text{prismatic}} < CRSS_{\text{pyramidal}}$  in magnesium and Mg-RE alloys at room temperature [12,26,27].

Sandlöbes et al. [28] reported that the limitation to mainly basal  $\langle a \rangle$  slip can lead to retention of a strong basal texture, and deformation by pyramidal slip would easily occur under this condition. However, there was no apparent basal texture in our as-cast alloy, as indicated above. Hence, the nature of dislocations in Fig. 3 are deduced to be basal  $\langle a \rangle$  slip, which has the lowest CRSS and is the common and easy mode of deformation in Mg-RE alloys at room temperature. In contrast, in the case of M2 alloy, the indentation did not affect the LPSO structure (Fig. 4a), but there were dislocations near the LPSO and indentation (Fig. 4b). They were characterized by short bent dislocations and long straight dislocations in the two-beam condition of  $g = [\bar{1}010]$ . However, only long straight dislocations were observed in the two-beam condition of  $g = [0002]$  (Fig. 4c). This implied that the second order pyramidal  $\langle c+a \rangle$  slip was activated during the deformation of M2 alloy with LPSO structure, besides the basal slip. A schematic diagram of dislocations in Fig. 4c(i) is presented in Fig. 4c(ii). As shown in Fig. 4c(ii), there are



four types of pyramidal  $\langle c+a \rangle$  slip dislocations, marked as A, B, C and D, respectively. It is proposed that in the case of the  $\langle c+a \rangle$  slip dislocation, there are generally four variants, i.e.  $b = 1/3[11\bar{2}3]$ ,  $b = 1/3[1\bar{1}2\bar{3}]$ ,  $b = 1/3[\bar{2}1\bar{1}3]$  and  $b = 1/3[\bar{2}113]$  [28]. The  $b = 1/3[11\bar{2}3]$  is easily activated in the form of climb-slip, which forms the climbing stage (identified by A). The  $b = 1/3[1\bar{1}2\bar{3}]$  is usually activated as straight edge dislocation, which forms a straight line in the material (identified by B). For  $b = 1/3[\bar{2}1\bar{1}3]$ , cross-slip generally occurs by this dislocation, which are mixed edge and screw dislocations, like the smooth “Z” shape (identified by C). For  $b = 1/3[\bar{2}113]$ , it is often dissociated as  $1/6[\bar{2}023] + 1/6[\bar{2}203]$ , which forms an elliptical shape in the straight slip line (identified by D). Thus, we envisage on comparing with M1 alloy without LPSO structure that non-basal slip systems are activated in M2 alloy because of the presence of LPSO structure.

During deformation, besides non-basal slip dislocations, a number of straight twins were also observed in the vicinity of the LPSO and indentation in M2 alloy, as presented in Fig. 5. The twins were confirmed to be  $\{10\bar{1}2\}$  deformation twins by the selected area diffraction pattern in Fig. 5b. It indicates that LPSO structure had an effect in introducing deformation twinning besides dislocation slip as a mechanism of deformation.

Basal dislocation slip occurred in both M1 and M2 alloys. However, the presence of LPSO structure in M2 alloy activated more slip systems (non-basal  $\langle c+a \rangle$  slip dislocations) and  $\{10\bar{1}2\}$  deformation twins. One possibility is that LPSO reduces the probability for initiation and propagation of cracks during deformation [29]. Second, the large size and high number of LPSO phases present along the grain boundaries (Fig. 1) effectively hinder the mobility of grain boundaries such that the LPSO phase leads to pile-up of dislocations. Moreover, an increase in stacking periodicity of LPSO can increase the critical resolved shear stress (CRSS) of the basal

plane [16], which was confirmed by first principle calculations [17]. Thus, the pyramidal plane is activated by LPSO phase to compensate for the limited deformation of the basal plane. It is proposed that the shear stress  $\tau$  for a perfect dislocation across the long ordered phase can be expressed as a power law [30,31]:

$$\tau = \frac{\gamma_0^{3/2}}{b} \left( \frac{4fr_s}{\pi T} \right)^{1/2} \quad (1)$$

where  $\gamma_0$  is the density of interfacial energy of the zone passed by a perfect dislocation,  $b$  is Burgers vector,  $f$  is volume fraction of long order phase,  $r_s$  is the radius of long order phase and  $T$  is tension of the dislocation line. According to equation (1), the shear stress  $\tau$  for the non-basal pyramidal dislocation  $b = 1/3 \langle 11\bar{2}3 \rangle$  is less than the basal dislocation  $b = 1/3 \langle 11\bar{2}0 \rangle$  and the pyramidal dislocation can easily pass the LPSO phase. Thus, pyramidal dislocations  $b = 1/3 \langle 11\bar{2}3 \rangle$  are activated by the formation of LPSO.

In regard to  $\{10\bar{1}2\}$  deformation twin, the mechanism of deformation twin is the intrinsic atomic movement. When a large load is applied along the basal plane, the deformation kinks are formed by a progressive rotation of the lattice by the avalanche generation of pairs of dislocations on the basal plane, as shown in Fig. 6, and these kinks accommodate the strain [32]. But in the alloy containing LPSO structures, when the kink bands approach the LPSO structures, the complicated stacking sequence of LPSO inhibits the deformation of kink bands. The atomic movement induced by the dislocations on the basal plane is impeded, and the atomic movement results in symmetrical deformation between kink bands and the matrix. As the load increases, the atoms cannot move forward anymore and assume an ordered arrangement, which finally transforms to deformation twins. If the kink bands occur in LPSO structures, it is easier to transform to deformation twins because of the original complicated stacking sequence of LPSO and symmetrical deformation of kink bands. This result is consistent with the opinion that

majority of the deformation bands with relatively large rotation angles are believed to be deformation twins [22].

From our TEM observations, we underscore the interaction between the LPSO structures and dislocations and deformation twins. In the alloy without LPSO structures many basal  $\langle a \rangle$  dislocations are present on the basal plane. The plastic deformation in polycrystalline Mg-RE alloys mainly occurs by basal slip, since the critical resolved shear stress (CRSS) of the basal slip system at room temperature is  $\sim 1/100$  in comparison to the non-basal slip systems [33,34]. On the contrary, a number of pyramidal  $\langle c+a \rangle$  dislocations and deformation twins were present in the alloy with LPSO structures. The underlying reason is that the non-basal slip is activated by the increased  $\text{CRSS}_{\text{basal}}$  and the deformation twin is activated and formed partially from the impeded kink bands.

The pyramidal dislocations and deformation twins can provide five deformation modes, which compensates for the restricted movement of dislocations near the grain boundaries with LPSO structures [35]. Thus, it is concluded that the LPSO phase contributes to the enhancement of strength and ductility in the alloy with LPSO structures leading to increase of the CRSS of the basal plane and increase in the number of slip systems such that non-basal slip and twinning are promoted.

#### 4. Conclusions

We have provided here an evidence of the relationship between LPSO structure and nanoscale deformation mechanism and mechanical properties, using an innovative approach of nanoscale deformation by nanoindentation combined with electron microscopy, which has not been previously addressed. Considering the activation of non-basal slip and deformation twin in the Mg alloy with LPSO structures, the LPSO plays a unique role in providing high strength and

high ductility in the alloy. First, the activation of non-basal slip promotes more homogeneous plastic deformation of grains and reduces the concentration of stress. Second, the deformation twins in the alloy with LPSO phase contributes to plasticity and LPSO phase strengthens the Mg alloys. Thus, the influence of the presence of the LPSO on deformation mechanism of Mg matrix leads to high strength and high ductility of M2 alloy.

### **Acknowledgements**

The authors gratefully acknowledge support from National Science Foundation for the acquisition of nanoindentation system through grant # DMR-MRI 1530891.

## References

- [1] Y. Kawamura, T. Kasahara, S. Izumi, M. Yamasaki, *Scr. Mater.* 55 (2006) 453–456.
- [2] E. Dogan, I. Karaman, G. Ayoub, G. Kridli, *Mater. Sci. Eng. A* 610 (2014) 220–227.
- [3] P. Trivedi, K.C. Nune, R.D.K. Misra, *Mater. Sci. Eng. A* 668 (2016) 59–65.
- [4] W.Q. Xu, N. Birbilis, G. Sha, Y. Wang, J.E. Daniels, Y. Xiao, M. Ferry, *Nat. Mater.* 14 (2015) 1229–1235.
- [5] K. Hantzsche, J. Bohlen, J. Wendt, K.U. Kainer, S.B. Yi, D. Letzig, *Scr. Mater.* 63(2010) 725–730.
- [6] K. Hagihara, A. Kinoshita, Y. Sugino, M. Yamasaki, Y. Kawamura, H.Y. Yasuda, *Acta Mater.* 58 (2010) 6282–6293.
- [7] E. Abe, Y. Kawamura, K. Hayashi, A. Inoue, *Acta Mater.* 50 (2002) 3845–3857.
- [8] Y.M. Zhu, A.J. Morton, J.F. Nie, *Acta Mater.* 58 (2010) 2936–2947.
- [9] T. Itoi, T. Seimiya, Y. Kawamura, M. Hirohashi, *Scr. Mater.* 51 (2004) 107–111.
- [10] A. Inoue, M. Matsushita, Y. Kawamura, *Mater. Trans.* 43 (2002) 580–584.
- [11] R. Chen, S. Sandlöbes, X. Zeng, *Mater. Sci. Eng. A* 682 (2017) 354–358.
- [12] W.B. Hutchinson, M.R. Barnett, *Scr. Mater.* 63 (2010) 737–740.
- [13] Y.M. Zhu, A.J. Morton, J.F. Nie, *Acta Mater.* 60 (2012) 6562–6572.
- [14] D. Egusa, E. Abe, *Acta Mater.* 60 (2012) 166–178.
- [15] Y. Muto, T. Shiraiwa, M. Enoki, *Mater. Sci. Eng. A* 689 (2017) 157–165
- [16] M. Matsuda, S. Ando, M. Nishida, *Mater. Trans.* 46 (2005) 361–364.
- [17] A. Datta, U.V. Waghmare, U. Ramamurty, *Acta Mater.* 56 (2008) 2531–2539.
- [18] K. Hagihara, N. Yokotani, Y. Umakoshi, *Intermetallics* 18 (2010) 267–276.

- [19] K. Hagihara, Y. Sugino, Y. Fukusumi, Y. Umakoshi, T. Nakano, *Mater. Trans.* 52 (2011) 1096–1103.
- [20] X. Shao, Z. Yang, X. Ma, *Acta Mater.* 58 (2010) 4760–4771.
- [21] J.K. Kim, S. Sandlöbes, D. Raabe, *Acta Mater.* 82 (2015) 414–423.
- [22] K. Kishida, A. Inoue, H. Yokobayashi, *Scr. Mater.* 89 (2014) 25–28.
- [23] K. Liu, L. L. Rokhlin, F. M. Elkin, *Mater. Sci. Eng. A* 527 (2010) 828–834.
- [24] K. Yamada, Y. Ohkubo, M. Shiono, *Mater. Trans.* 47 (2006) 1066–1070.
- [25] R.D.K. Misra, V.S.A. Challa, P.K.C. Venkatsurya, Y.F. Shen, M.C. Somani, L.P. Karjalainen, *Acta Mater.* 84 (2015) 339–345.
- [26] M.R. Barnett, Z. Keshavar, X. Ma, *Metall. Mater. Trans. A* 37 (2006) 2283–2293.
- [27] M.R. Barnett, *Metall. Mater. Trans. A* 34 (2003) 1799–1806.
- [28] S. Sandlöbes, S. Zaeferrer, I. Schestakow, S. Yi, R. Gonzalez-Martinez, *Acta Mater.* 59 (2011) 429–439.
- [29] T. Honma, T. Ohkubo, S. Kamado, *Acta Mater.* 55 (2007) 4137–4150.
- [30] Z.H. Lai, *Crystal defects and mechanical properties of metals*, Metallurgical Industry Press, Beijing (CHN), 1984.
- [31] C. T. Sims, W. C. Hagel, *The Superalloys*, John Wiley & Sons Inc. Press, New York (USA) 1972.
- [32] J.B. Hess, C.S. Barrett, *Trans. Am. Inst. Min. Met. Eng.* 185 (1949) 599–606.
- [33] A. Akhtar and E. Teghtsoonian: *Acta Metall.* 17 (1969) 1351–1356.
- [34] S. Miura, S. Yamamoto, K. Ohkubo and T. Mohri: *Mater. Sci. Forum* 350–351 (2000) 183–188.

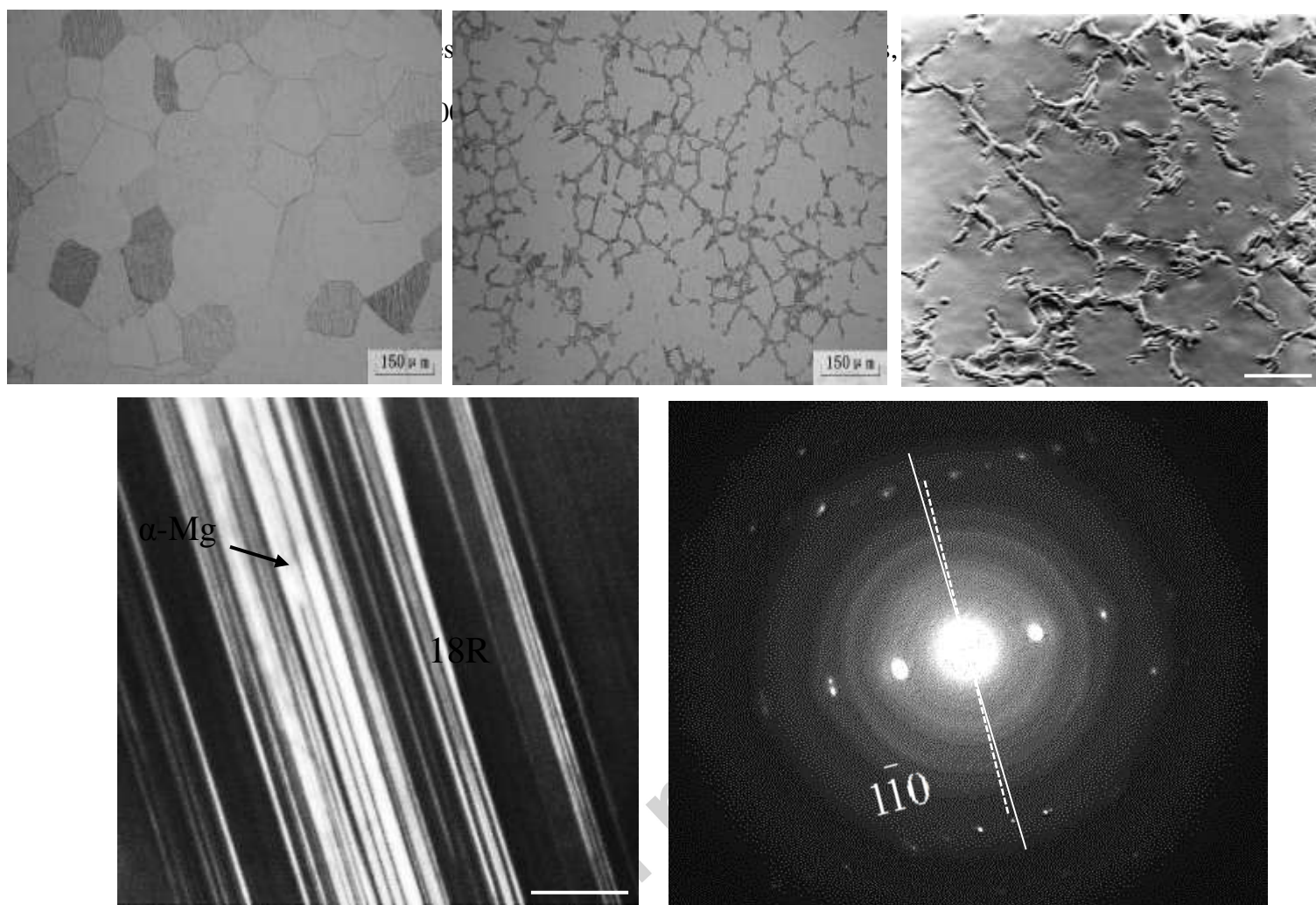


**Figure 1. (a) Light micrograph of M1 (free of LPSO) alloy and b(i) light and b(ii) SEM micrographs of M2 (LPSO-containing) alloy, c(i) TEM bright field image of the secondary phase (LPSO) and c(ii) the corresponding selected area diffraction pattern.**

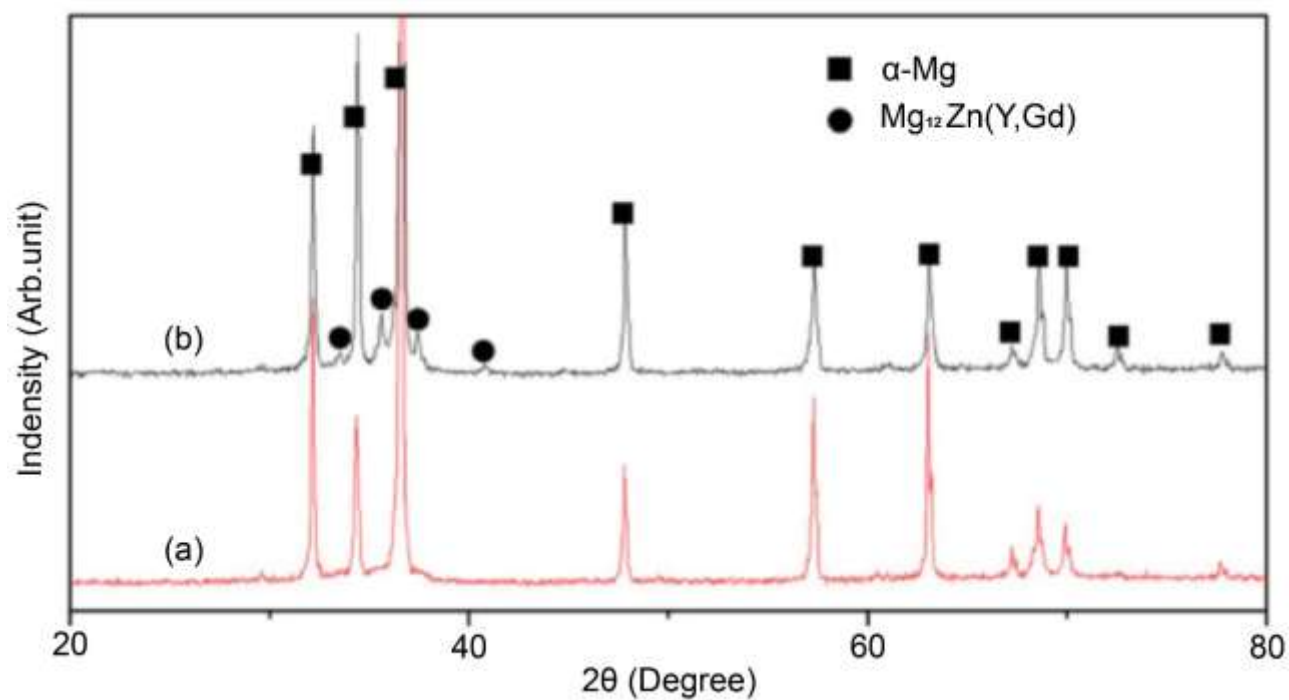
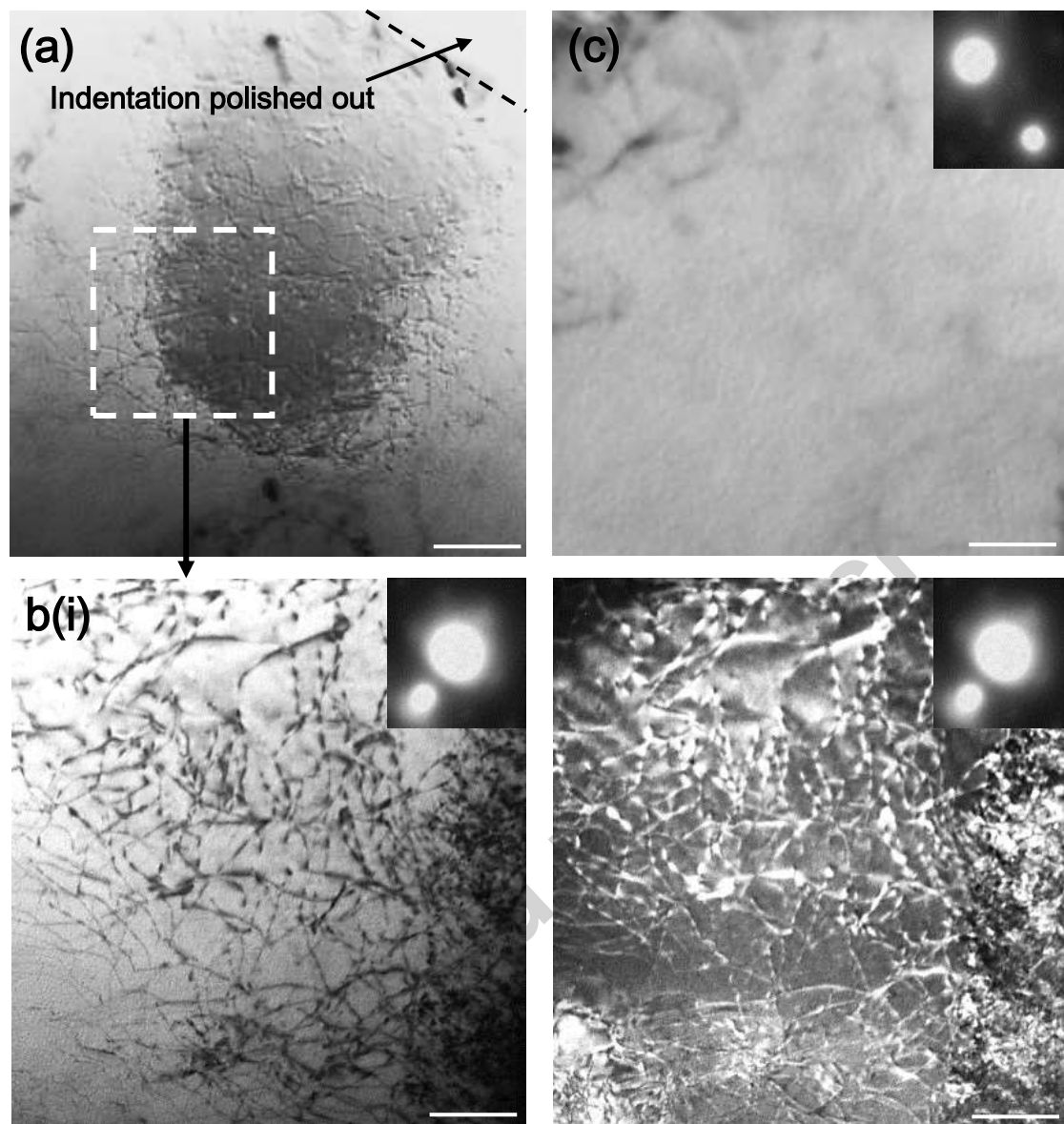
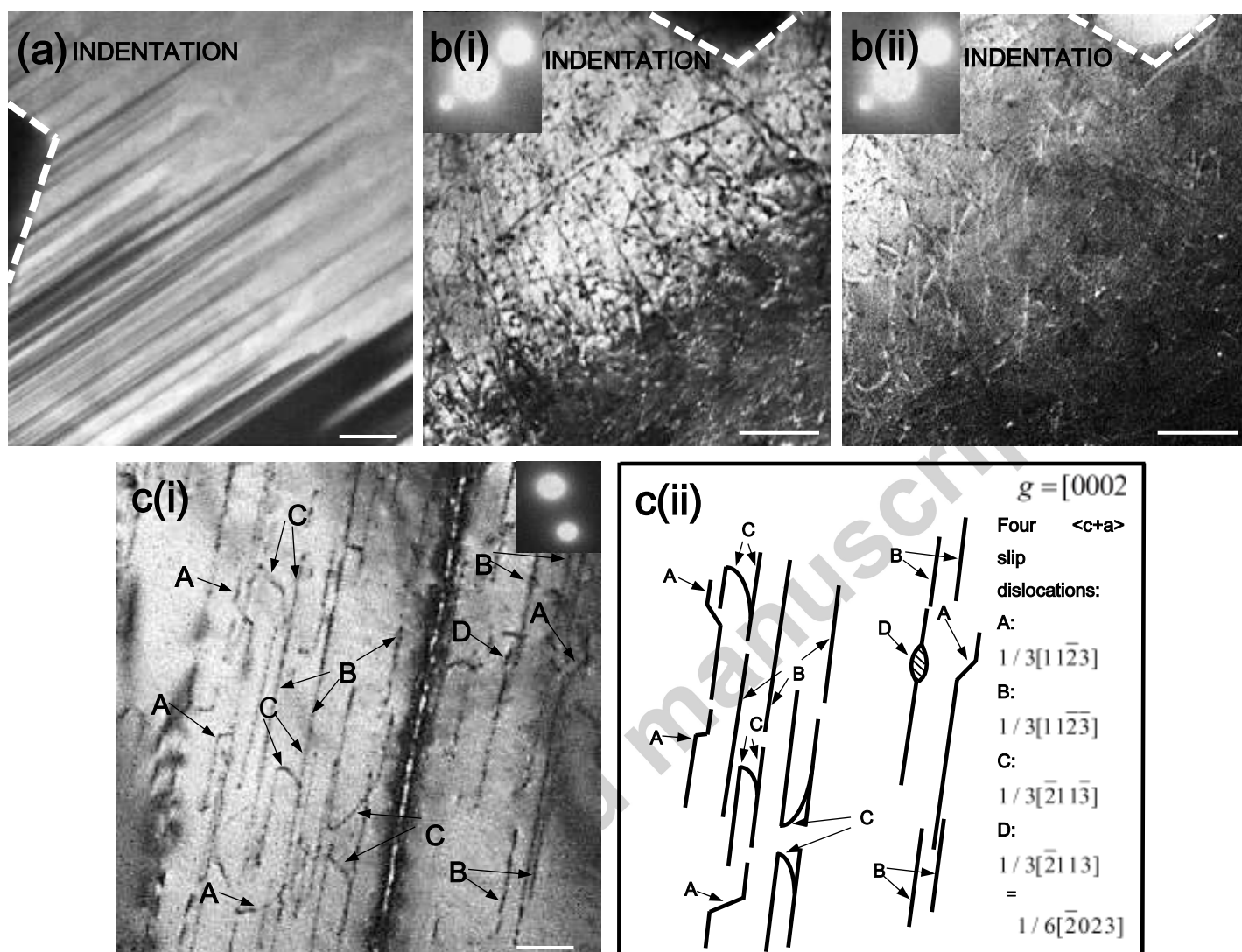


Fig. 2. X-ray diffraction patterns of alloys (a) M1 alloy, (b) M2 alloy





**Figure 3.** TEM micrographs of M1 (free of LPSO) alloy. (a) An area surrounding the indentation, (b) high magnification of zone B in b(i) bright field and b(ii) dark field in the two-beam condition of  $g = [10\bar{1}0]$ , (c) high magnification of zone B in bright field in the two-beam condition of  $g = [0002]$ .



**Figure 4. TEM micrographs of M2 (LPSO-containing) alloy. (a) An area of LPSO structure surrounding the indentation, (b) an area near LPSO and indentation in b(i) bright field and b(ii) dark field in the two-beam condition of  $g = [\bar{1}010]$ , c(i) an area surrounding the indentation in bright field in the two-beam condition of  $g = [0002]$  and c(ii) schematic diagram of dislocations in c(i).**

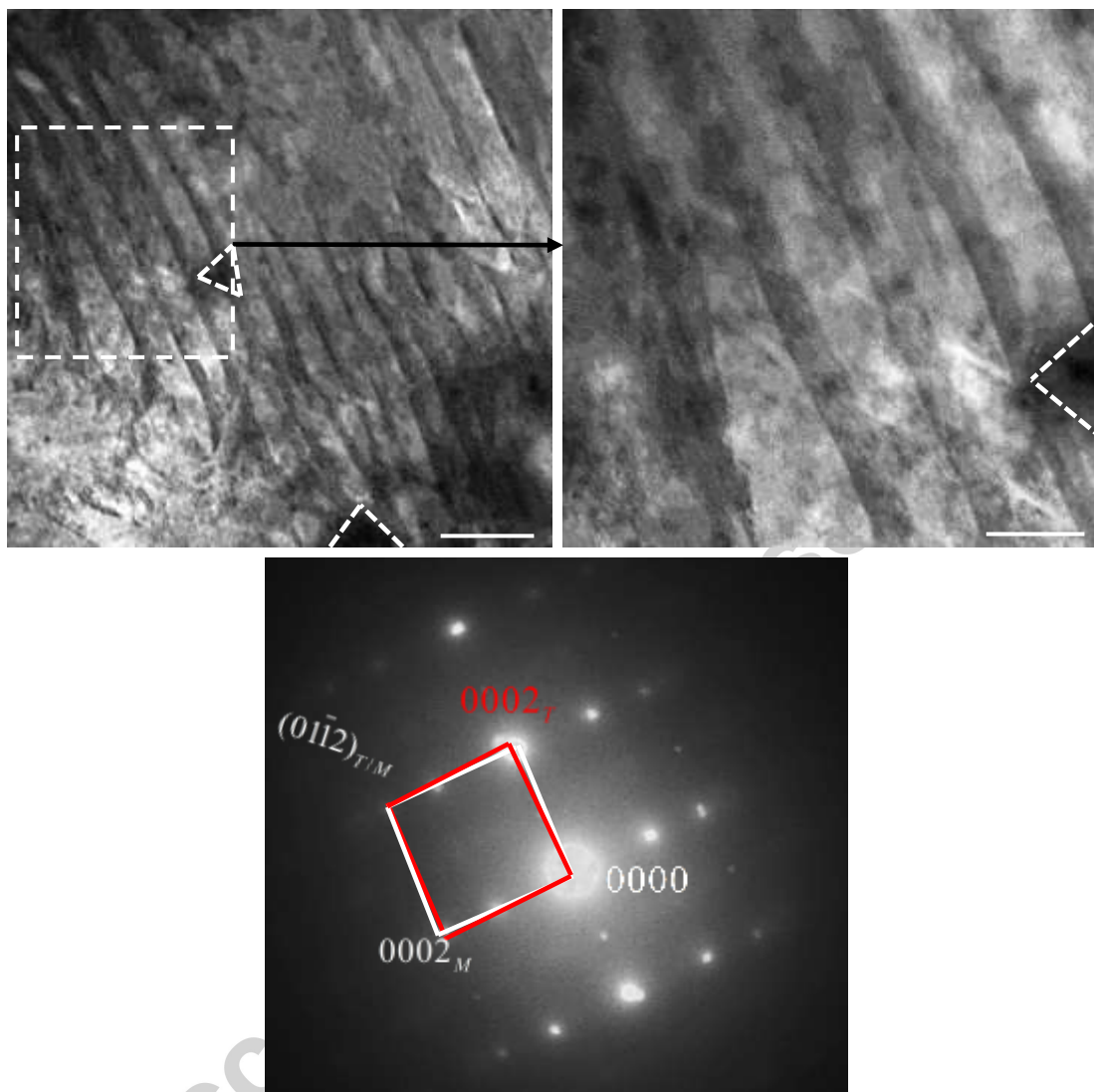


**Figure 5. TEM micrographs of the area near LPSO and indentation in M2 (LPSO-containing) alloy. a(i) Low magnification, a(ii) high magnification, and (b) selected area diffraction pattern of twinned region in a(ii).**

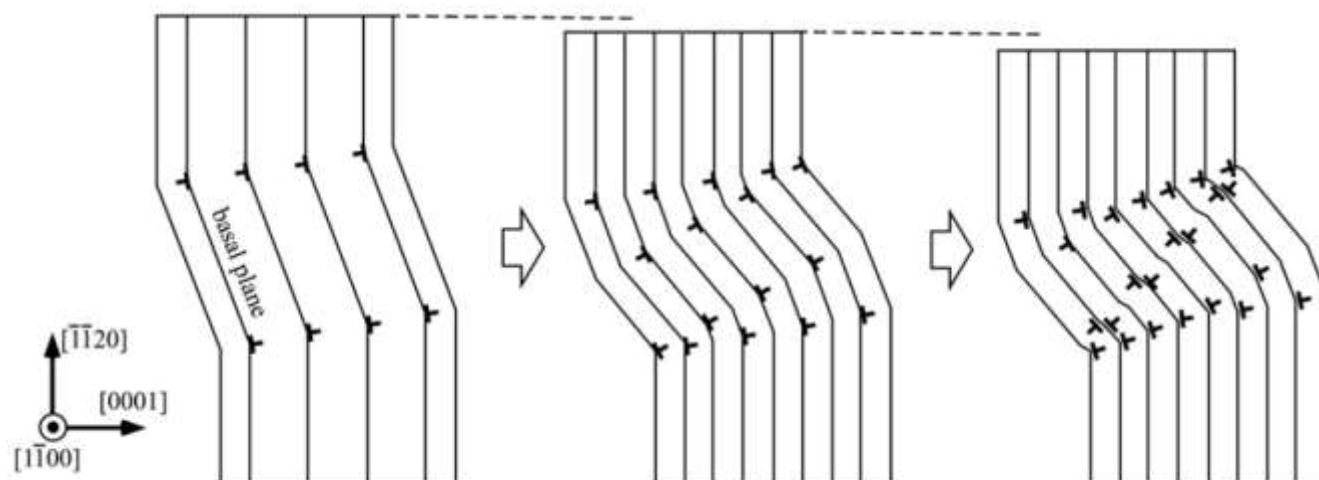


**Figure 6.** Formation of a deformation kink induced by the mobility of dislocations on the basal plane [32].

### Table captions

Table 1. Mechanical properties of magnesium-rare earth alloys at room temperature.

Alloy	YS (MPa)	UTS (MPa)	Elongation (%)
M1 (without LPSO)	32	65	15
M2 (with LPSO)	131	240	21.4